NRC·CNRC

NRC Publications Archive
Archives des publications du CNRC

Practical approach to enhance compatibility in silicon/graphite composites to enable high-capacity Li-ion battery anodes

Naboka, Olga; Yim, Chae-Ho; Abu-Lebdeh, Yaser

This publication could be one of several versions: author's original, accepted manuscript or the publisher's version. / La version de cette publication peut être l'une des suivantes : la version prépublication de l'auteur, la version acceptée du manuscrit ou la version de l'éditeur.
For the publisher's version, please access the DOI link below./ Pour consulter la version de l'éditeur, utilisez le lien DOI ci-dessous.

Publisher's version / Version de l'éditeur:
https://doi.org/10.1021/acsomega.0c04811
ACS Omega, 6, 4, pp. 2644-2654, 2021-01-19

NRC Publications Archive Record / Notice des Archives des publications du CNRC :
https://nrc-publications.canada.ca/eng/view/object/?id=6b0f361c-dc22-45af-a196-612f99cc31c6
https://publications-cnrc.canada.ca/fra/voir/objet/?id=6b0f361c-dc22-45af-a196-612f99cc31c6

Access and use of this website and the material on it are subject to the Terms and Conditions set forth at
https://nrc-publications.canada.ca/eng/copyright
READ THESE TERMS AND CONDITIONS CAREFULLY BEFORE USING THIS WEBSITE.

L'accès à ce site Web et l'utilisation de son contenu sont assujettis aux conditions présentées dans le site
https://publications-cnrc.canada.ca/fra/droits
LISEZ CES CONDITIONS ATTENTIVEMENT AVANT D'UTILISER CE SITE WEB.

Questions? Contact the NRC Publications Archive team at PublicationsArchive-ArchivesPublications@nrc-cnrc.gc.ca. If you wish to email the authors directly, please see the first page of the publication for their contact information.

Vous avez des questions? Nous pouvons vous aider. Pour communiquer directement avec un auteur, consultez la première page de la revue dans laquelle son article a été publié afin de trouver ses coordonnées. Si vous n'arrivez pas à les repérer, communiquez avec nous à PublicationsArchive-ArchivesPublications@nrc-cnrc.gc.ca.

National Research Council Canada | Conseil national de recherches Canada

Canada

A practical approach to enhance compatibility in silicon/graphite composites to enable high capacity Li-ion battery anodes

Olga Naboka, Chae-Ho. Yim, Yaser Abu-Lebdeh*

*Corresponding author: Yaser.Abu-Lebdeh@nrc-cnrc.gc.ca

National Research Council Canada

1200 Montreal Road, Ottawa, Ontario K1A 0R6, Canada

Tel: 1 613 949 4184

Abstract

There is an urgent need to improve the energy density of Li-ion batteries to enable mass-market penetration of electric vehicles, grid-scale energy storage and next generation consumer electronics. Silicon-Graphite composites are currently the most plausible anode material to overcome capacity limit of graphite or poor cycling performance of silicon. One serious and unrecognized limitation to the use of the composite as an anode is the incompatibility of hydrophobic (natural) graphite with the hydrophilic Si which adversely affects battery performance. Herein, we report a novel, practical approach to modify the graphite resulting in the formation of a hard carbon coating and graphene sheets that give rise to higher compatibility with Si nanoparticles in the composite. Electrochemical and battery testing of the composite (10 wt% Si) anode shows higher reversible capacity (10 % at C/12 and 20% at C/2) than the composite with unmodified graphite reaching ~ 600 mAh/g with 95% retention after 100 cycles. The enhanced battery performance is explained by the uniform distribution of Si nanoparticles at the modified

graphite surface due to the presence of graphene conductive networks and thin, oxygen-rich, amorphous carbon layer on the surface of graphite particles, as evidenced by TEM images and XPS spectra. This work provides a new approach to prepare graphite compatible materials that can work with hydrophilic components other than silicon for various applications other than batteries.

Keywords

Silicon nanoparticles, Li-ion batteries, hard carbon, Si/graphite composite

1. Introduction

Silicon has been recognized as a prospective anode material for Li-ion batteries due to its extraordinary theoretical capacity (4200 mAh/g) for more than 20 years [1] and interest in it is constantly growing due to the ever-increasing demand for higher energy batteries. There are a lot of reports on Si achieving practical capacity of up to 3000 mAh/g [2-4], but Si-based anodes are yet to be commercialized since cycle life and performance in full cells are poor. For instance most reports show that very high capacity values were obtained when using high amount of inactive materials (binder and conductive additive can reach up to 50% of total electrode weight) and low electrode loading (<1mg/cm^2) which cannot be adopted by industry [2-5]. The other major problem is poor reproducibility caused by using the "in-house" made silicon with various morphologies (e.g. silicon nanowires [3,6], silicon nanoparticles [7], porous silicon [8,9], silicon nanosheets [10], silicon nanotubes [11], just to name a few); or commercial silicon available in low-batches only [4]. However, it is obvious that only cheap commercial silicon with reproducible properties could be of interest for battery industry.

Bare Si undergoes fast capacity fade due to its pulverization as a result of huge volume changes during cycling, formation of excessive amount of SEI, incomplete delithiation due to high polarization, and loss of contact with conductive additives and current collector [5, 12, 13]. The main approaches to overcome this are the use of Si nanomaterials instead of micro-sized Si in order to minimize the stress-induced fracture during cycling, additional reinforcing of Si to protect its integrity, and providing Si with more intimate contact with conductive additives [5, 12, 14]. Reinforcing strategies are mainly devoted to reinforcing the electrode coating by using binders and conductive supports (such as graphene) forming flexible yet mechanically stable 3-D network [2, 4, 5, 15, 16] or reinforcing Si by applying protective coating on its surface [17-21], including carbon coating [3, 5, 8, 9, 17, 19, 20, 22-26]. However, efforts on stabilizing Si capacity usually end up with substantial increase in the final electrode price and therefore loss of practical value. Another way to stabilize the electrode during cycling is to use Si in a composite with graphite at low content (e.g. <30 wt%) and with compatible binder, thus the total electrode volume expansion is limited and good contact is provided by electrically conductive agents and graphite [27-30]. We have recently shown that only 17 % increase in practical energy density can be achieved when using 10-25% of Si in electrode formulations [30]. Such approach offers transitional and more practical solution when it comes to implementation of Si into the full cells since anode capacity of modern industrial Li-ion batteries is limited by the capacity of cathode (2.5-3.5 mAh/cm^2) and maximal current density <4mA/cm^2 to avoid Li-plating [31-32] which means that Si-only anodes are not practical.

Good performance of Si/graphite composites can be expected only in the case of good compatibility between the Si nanoparticles and graphite. However, graphite as a highly hydrophobic material does not favor a good contact with the hydrophilic surface of Si (fig. 1 a).

This problem could be solved in two ways: either by modifying the surface of Si (e.g. with carbon coating) (fig. 1 b) or by modifying the surface of graphite (fig. 1 c). The latter approach is more practical and relevant to industry as the modification of relatively cheap and abundant graphite is obviously much more cost-effective than the modification of an already very pricy nano-silicon material.

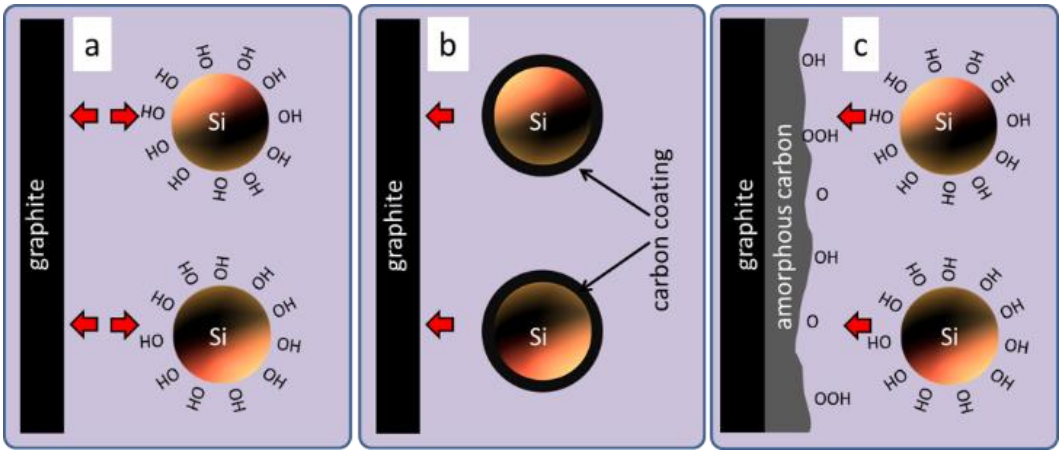

Fig.1 Schematic of the interaction between surfaces of Si nanoparticles and graphite microparticles: (a) bare silicon nanoparticles and native graphite, (b) carbon-coated Si nanoparticles and native graphite; (c) native silicon nanoparticles and graphite coated with oxygen-rich amorphous carbon.

Graphite used in Li-ion batteries is typically modified with a carbon layer derived from pitch to decrease surface area and functionalities [33]. Such modification however does not necessarily mean good compatibility with Si nanomaterials since pitch-derived carbon is expected to be highly hydrophobic too, so new graphitic materials which are suitable to be used together with Si should be developed. In a previous work we modified graphite with graphene layers by liquid exfoliation of graphite in Na carboxymethyl cellulose (NaCMC) solutions and it enhanced the capacity of Si

nanopowder [34]. In the composite, graphene was assumed to form a conductive network which was able to accommodate volume changes of silicon during cycling.

In the present work, we besides partially exfoliating graphite in order to introduce small amount of graphene sheets at the surface we further modified it with cellulose-derived hard carbon. In order to simplify the whole process and make it easily scalable, the same cellulose polymer was chosen to be both the graphite exfoliant and the precursor for carbon coating. Besides, effective graphene formation and its stabilization by cellulose derivatives are known to yield carbon with high oxygen content [35, 36] (so called "hard carbon" [33]) which is expected to favor Van der Waals interactions with Si nanoparticles. However, even though NaCMC proved to be an excellent graphite exfoliant [34] it was not selected in the present work since Na_2CO_3 forms during heat treatment of NaCMC which is undesirable for application in Li-ion battery anodes. Instead, non-ionic cellulose derivatives – methyl cellulose (MC), and ethylcellulose (EC), were applied in this work. The modification was performed in two stages: first graphite was partially exfoliated by sonication in solutions of methylcellulose (MC) in water or ethylcellulose (EC) in acetone, and then the obtained polymer/graphene/graphite material was carbonized yielding hard carbon-coated graphene/graphite material. The obtained materials were combined with commercial Si nanoparticles in composite anode formulations for Li-ion batteries and showed superior cycling compared to unmodified natural graphite.

2. Results and discussion

2.1 Modification of graphite samples

Fig. 2 shows a schematic of the surface modification of natural graphite with cellulose-derived carbon. The process is simple and straightforward and does not require special equipment (e.g.

CVD or rotating furnace). Moreover, decomposition of cellulose derivatives is not expected to lead to formation of dangerous compounds (e.g. halogenated organic compounds or polycyclic aromatic compounds) [38] which is highly desired because of reduced environmental footprint.

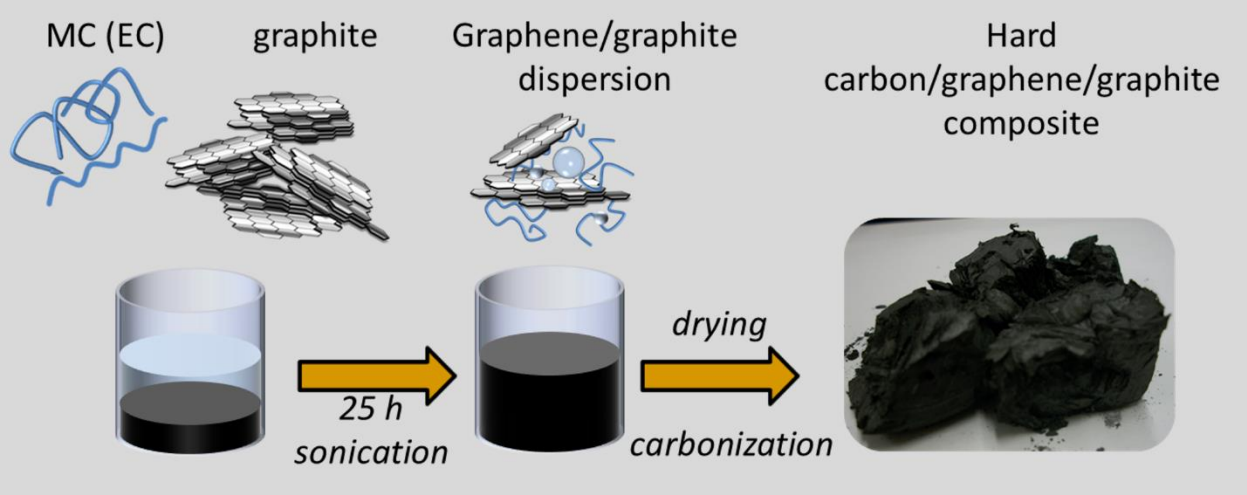

Fig.2 Schematic of surface modification of natural graphite with polymer-derived carbon.

Sonication-assisted exfoliation of graphite in EC or MC solutions resulted in the formation of graphene/graphite dispersions. Concentration of graphene in the supernatant obtained after centrifugation was measured to be 1.42 mg/ml for graphite exfoliated in water solution of MC and 2.6 mg/ml for graphite exfoliated in acetone solution of EC. The value for MC is close to that obtained for sonication-assisted exfoliation of graphite in NaCMC (1.36 mg/ml) reported by us previously [34]. Concentration of graphene obtained after exfoliation in EC solution is almost two times higher than that in MC solution under the same sonication condition. Such a high yield rise might be caused by few factors, such as the use of the non-polar solvent acetone or the hydrophobic properties of EC, which favor penetration of polymers between graphite sheets. We think that further optimization of polymer molecular weight and concentration could lead to even higher

concentration of the final graphene, as it changes the viscosity of solution which in turn can affect stabilizing properties of polymers; but this is out of the scope of this work.

Carbonization of dried polymer/graphene/graphite composites resulted in hard carbon-coated graphene/graphite composites. TEM of carbonized samples besides non-exfoliated graphite flakes revealed the presence of multilayered graphene covered with amorphous carbon (Fig. 3 a, b). The lateral size of flakes is 100-500 nm which is typical for sonication-derived graphene [34, 37, 39].

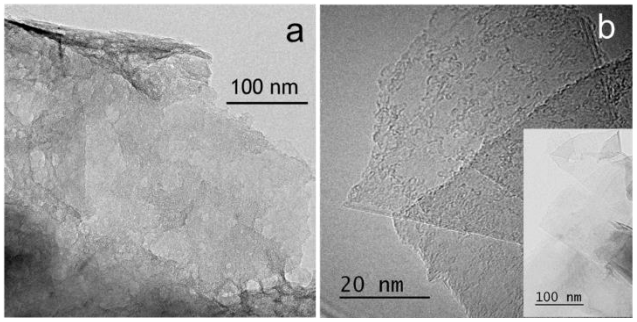

Fig. 3 TEM images of graphene (A, B) obtained by exfoliation of graphite with MC

SEM of carbonized graphitic samples (Fig. 4) has shown that morphology of exfoliated materials resemble that of starting graphite sample. This is expected since the graphene yield is only around 1.4% for MC-assisted exfoliation and 2.6% for EC-assisted exfoliation (The yield was approximately estimated assuming that volume of solvent is equal to the volume of solution and dispersion). A closer look at the composites reveals that the surface of carbonized samples is rough and contains some coating which is not present at the surface of natural graphite. The coating is expected to consist of amorphous carbon formed from carbonized polymer. However coating is not evenly distributed throughout the graphite surface. Morphology of surface coating of sample 25EC/gr differs from morphology of surface coating of samples 25MC/gr and MC/gr which is most probably caused by hydrophobic properties of EC. MC as a water-soluble, hydrophilic

polymer adsorbs in different ways onto graphite than the hydrophobic EC. Thermal degradation of EC and MC proceeds in somewhat different ways too which was demonstrated by TGA (Fig. 5a): MC was thermally stable up to 250^{o}C and gave carbonization yield at 8.2 wt% after 1 hour at 800^{o}C; while EC started to decompose as early as 150^{o}C and its carbonization yield was two times less – only 3.7 wt%.

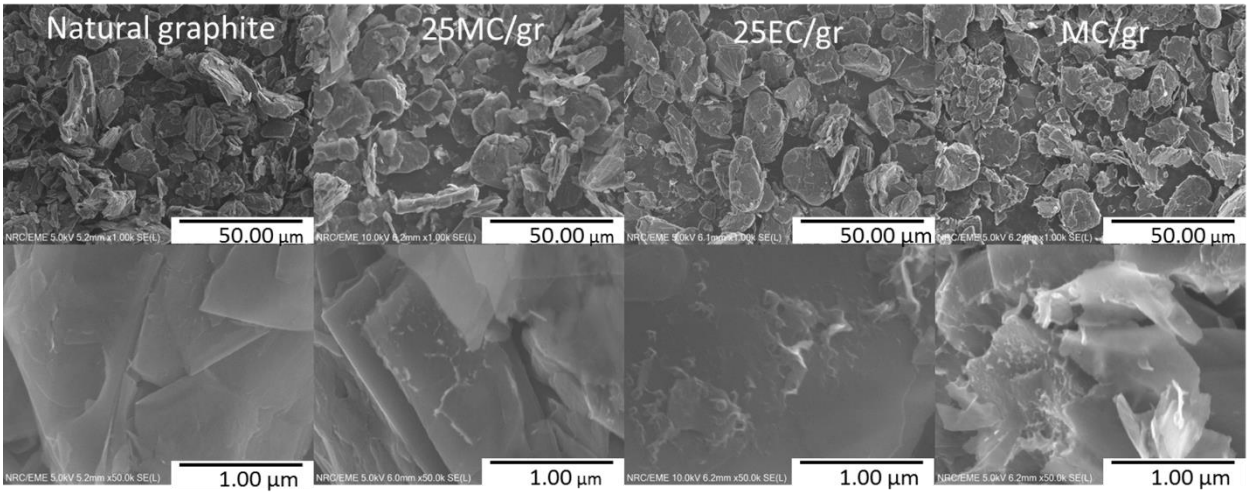

Fig. 4 Morphology of graphitic samples. Natural graphite, MC-derived graphite and EC derived graphite.

Based on TGA of bulk polymers, the amount of amorphous carbon in modified graphite was estimated to be ~2.3% for both 25MC/gr and MC/gr and ~1.1% for 25EC/gr, assuming that the yield of carbonization in the graphite containing composites is the same as in the bulk MC or EC (Fig. 5a). Such low hard carbon content is beneficial from the point of view of making active electrode materials since hard carbon usually suffers from high irreversible capacity losses [33]. XRD of obtained graphitic samples (Fig. 5b) are all typical for XRD of highly crystalline graphite – they have typical, sharp 002 peak (26.54˚, d_{002}=3.36). Broadening of 002 peak was not observed for modified samples which is most probably because of low graphene and amorphous carbon content and very high intensity of 002 peak of non-exfoliated (intact) graphite.

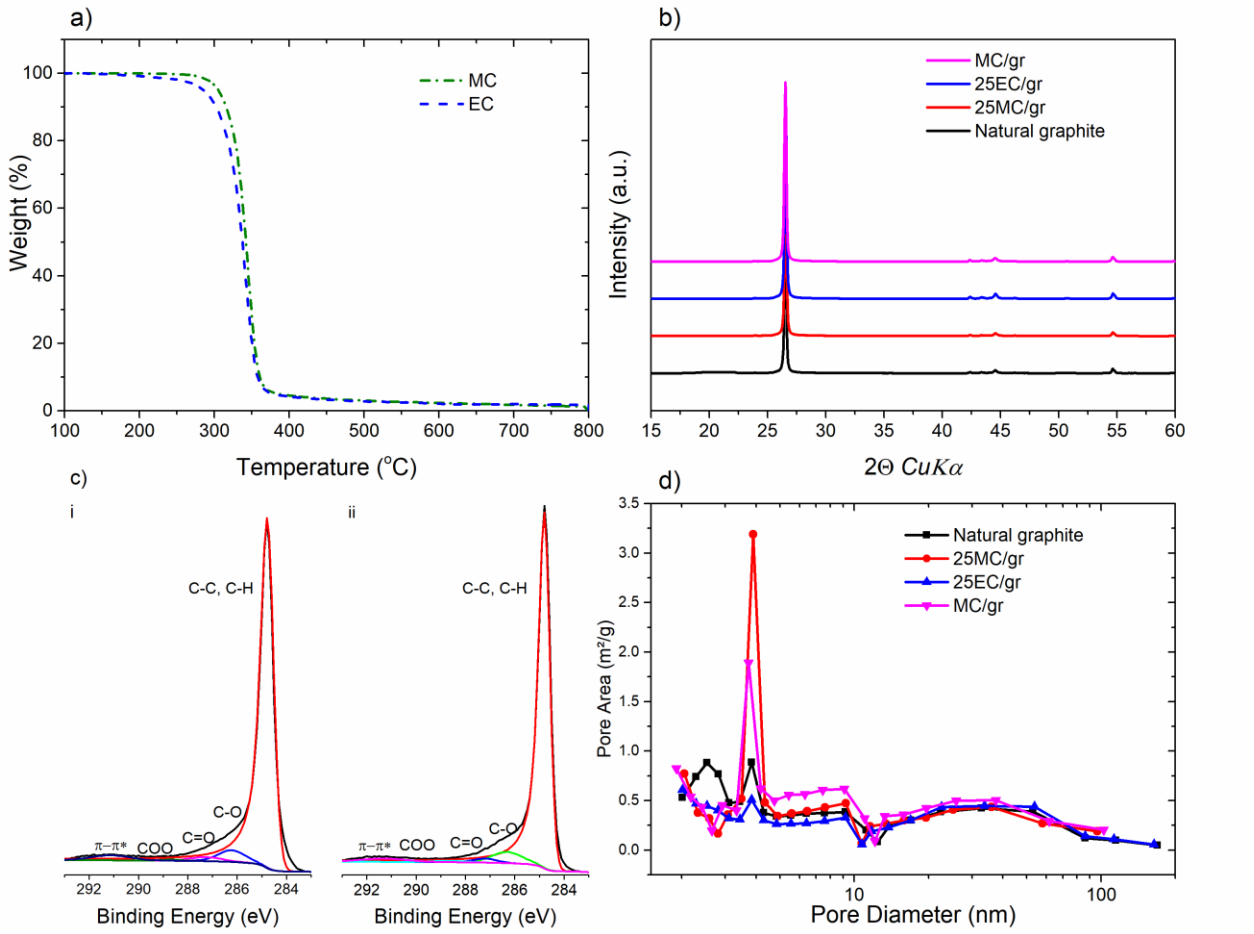

Fig. 5 a) TGA scans of MC and EC in nitrogen flow, b) XRD patterns of natural graphite and exfoliated carbonized composites, c) C1s XPS spectra of 25MC/gr graphite (i) and graphite (ii), d) Pore size distribution of graphite samples. Note that curves were offset by Y axis for 0.3-1.2 m^2/g to make them legible.

XPS technique was used to assess the surface composition of composite samples. Interestingly, it was found that surface oxygen content is higher in the native graphite sample, than in modified samples (Table 1). Instead of its expecting rise through the formation of oxygen-rich carbon the total amount of surface oxygen decreased by half. This is most probably caused by loss of oxygen functionalities that are present at the edges of native graphite during heat treatment [40, 41].

Moreover, the reducing atmosphere formed by the products of polymer decomposition can further decrease the amount of oxygen-containing species. Instead of oxygen inherent to native graphite, oxygen functionalities originating from cellulose derivatives are incorporated into the amorphous carbon. Since oxygen-rich amorphous carbon is present both on the edges and basal planes of graphite particles we expect homogeneous distribution of Si nanoparticles and binder in the electrode formulation. Individual C1s XPS spectra of samples are asymmetric and are widened towards higher binding energy which is typical for graphite [40, 42]. C1s spectra of starting graphite and 25MC/gr were shown on Fig. 5c as an example. Spectra were resolved to individual components which were assigned to C-C/C-H (around 284.7 eV), C-O (around 285.9-286.3 eV), C=O (287.2-287.5 eV), COO (288.7 – 289.3 eV) and π-π* shake-up (291.0-291.3 eV) [40, 43]. There is no obvious difference in the C1s spectra shape and features between natural graphite sample and modified samples so it is impossible to tell by XPS whether oxygen was inherent to graphite or cellulose-derived carbon (Fig. 5c).

Table 1 Surface properties of graphite samples

sample	Surface composition by XPS at%		Surface area (BET) m^2/g	Micropore area m^2/g
	C	O		
Natural graphite	98.6	1.4	8.2	0.8
25MC/gr	99.3	0.7	16.6	6.4
25EC/gr	99.3	0.7	6.7	0.02
MC/gr	99.0	1.0	9.7	1.1

It was found from the low-temperature nitrogen adsorption profile that starting natural graphite has quite a high specific surface area – 8.2 m^2/g (table 1) which might be a reason for high oxygen

content as oxygen functionalities accumulate mainly on the edges of flakes (see Fig. S1 for Nitrogen adsorption/desorption isotherms). Modified graphite samples did not show significant surface area increase which was expected if one takes into account the low graphene yield. Besides graphene formation, other processes that can affect the surface area during heat treatment of modified graphite are removal of disordered carbon fragments which typically present in natural graphite, re-stacking the graphene layers and formation of carbon from polymeric exfoliants. While first two processes lead to decreasing the specific surface area, the last one contributes to surface area increase – formed amorphous carbon not only prevents graphene layers from re-stacking but also may possess its own porosity. The highest specific surface area was observed in 25MC/gr (16.6 m^2/g) which is most probably caused by steric stabilization of exfoliated graphene sheets with amorphous carbon which contributes also to the total surface area through formation of micro- and meso-pores. Our assumption that MC is the main source of meso- and micro-porosity is supported by the fact that both exfoliated and non-exfoliated samples, 25MC/gr and MC/gr, have very similar pore size distribution with majority of pores around 3.6-3.9 nm (Fig. 5d). In contrast to MC-modified samples, EC-modified sample (25EC/gr) has even lower surface area than natural graphite – 6.7 m^2/g and demonstrates the absence of microporosity, which is most probably caused by the low amount of amorphous carbon (due to low carbonization yield of EC) which is unable to stabilize exfoliated graphite (Table 1, Fig. 5d).

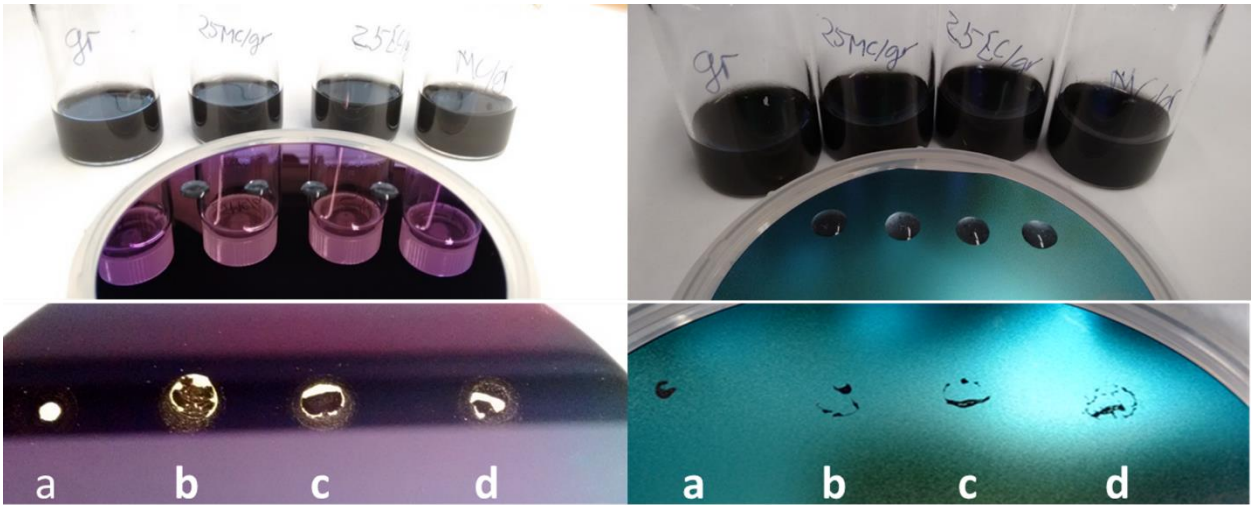

Fig. 6 Photos of drops of water:ethanol dispersions of natural (a) and modified graphite samples (b - 25MC /gr, c – 25EC/gr, d – MC/gr) on the oxidized Si wafer. Left column – polished side of wafer; right column– non-polished side of wafer.

To test our assumption that modified graphite samples show better compatibility with Si surface, we prepared modified graphite dispersions in water-ethanol mixtures (2:1 water:ethanol ratio), sonicated them for 15 minutes and placed 50 µl drops of dispersions onto the surface of oxidized Si wafers (both polished and non-polished side). The graphite distribution on the surface of wafer was compared after liquid evaporation (Fig. 6). The reason why oxidized wafer was used instead of the non-oxidized was to simulate the expected presence of native silicon dioxide on the surface of silicon nanoparticles [4]. Natural graphite showed the most compact accumulation with very little graphite amount on the initial perimeter of drop which point to little or no interaction between graphite and silicon/silicon dioxide surface. In contrast, all three modified graphite samples showed much bigger stain diameter close to the initial drop diameter and more even surface distribution. These qualitative observations demonstrate improved compatibility of modified

graphite samples with silicon dioxide surface comparing to that of natural graphite which makes our samples to be prospective for Si/graphite composite anodes.

2.2 Performance of composites in Li-ion batteries.

Modified graphitic samples were tested as active electrode materials for Li-ion battery anodes (Fig. 7). Natural graphite shows pronounced conditioning effect. It has very low first-cycle capacity – 83 mAh/g, only 64% initial coulombic efficiency and reaches its maximum capacity of 360 mAh/g only after 75 cycles. Such behavior might be a sign of bad compatibility with hydrophilic NaCMC binder as otherwise it shows stable cycling with PVDF binder (see S2 on cycling behavior with PVDF binder). Modified graphite samples show much higher initial coulombic efficiency (25MC/gr – 82.6%, 25EC/gr – 86.7%, MC/gr – 83.7%) and more stable cycling which indicates improved compatibility with binder. We can also expect that modified carbon would have stronger interaction with Si nanoparticles. Among modified graphite samples the best performance is observed for 25EC/gr – it reaches 350 mAh/g by 40 cycles and has the lowest irreversible capacity. These results are in line with the modification outcome – decrease of surface area and total micro-porosity (Table 1) and very low amorphous carbon content. 25MC/gr and MC/gr both show

continuous capacity increase with cycling that might be a sign of graphite exfoliation during repeated lithiation-delithiation which makes graphite basal planes more accessible for Li ions.

Fig. 7 Cycling performance of modified graphite samples in Li-ion half cells (active material loading 6.5-6.7 mg/cm^2) at C/12 rate.

The Silicon chosen for preparation of electrodes in this work consists of spherical particles with

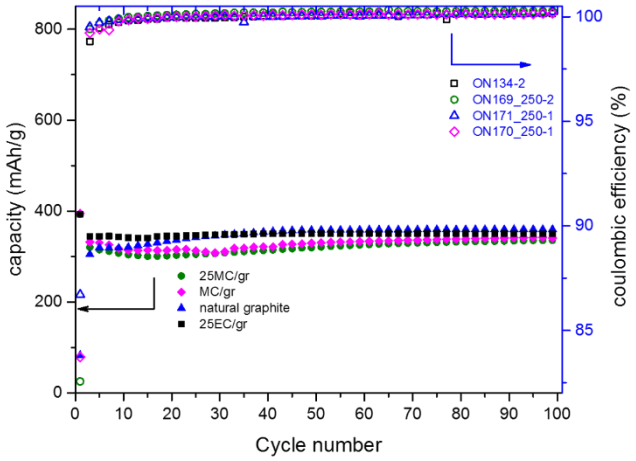

broad size distribution ranging from 30 nm to 200 nm (Fig. 8 a, b). Silicon particles contain a thick oxide layer (10-20 nm) that can be seen both in bright-field TEM as amorphous outer part of particles (Fig. 8 b) and in EELS profile showing the presence of oxygen at the surface of particles (Fig. 8 c). This is consistent with observations of C.Erk et al. that a thick oxide layer always exist at the surface of silicon of the same origin [4].

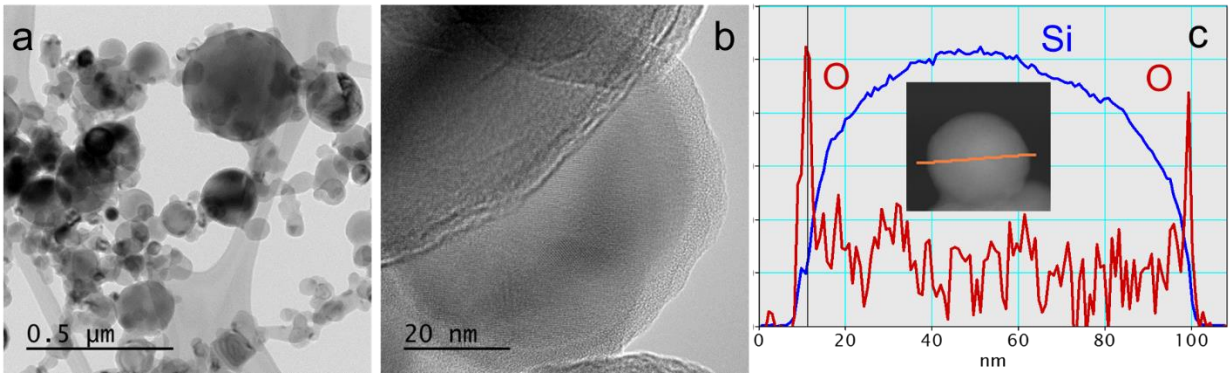

Fig. 8 TEM image of silicon nanoparticles used in our work: a, b – bright field TEM image, c – EELS profile of Si nanoparticle with its dark field image.

As seen on SEM images (Fig. 9) composite anodes prepared with 10% of nanosilicon with modified graphite samples demonstrate more uniform Si distribution than anode containing unmodified natural graphite as expected. Higher magnification SEM images of anodes with exfoliated graphite samples (25MC/gr and 25EC/gr) show graphene flakes "wrapping" silicon particles (Fig. 9, lower row). We expect that it can even provide extra mechanical support and electronic conductivity for Si composites. This is very important during delithitation as it minimize the increase in resistance and polarization which are the main reasons of incomplete delithiation [13].

Table 2 Cycling behavior of Si containing composites

graphite	Loading mg/cm^2	Theoretical capacity mAh/g	Initial coulombic efficiency %	Maximal capacity of composite	Maximal capacity of graphite mAh/g	Maximal nominal capacity of Si mAh/g	Capacity retention (100 cycles) %

Natural graphite	6.5	818	49.6	401	360	712	82
	3.2	818	83.0	550		1991	90
25MC/gr	6.7	812	82.9	480	336	1587	77
	2.8	812	83.1	565		2326	95
25EC/gr	6.6	803	82.3	471	351	1417	99
	3.2	819	85.2	543		1996	95
MC/gr	6.5	819	83.3	465	341	1328	92
	2.9	819	83.2	559		2134	94

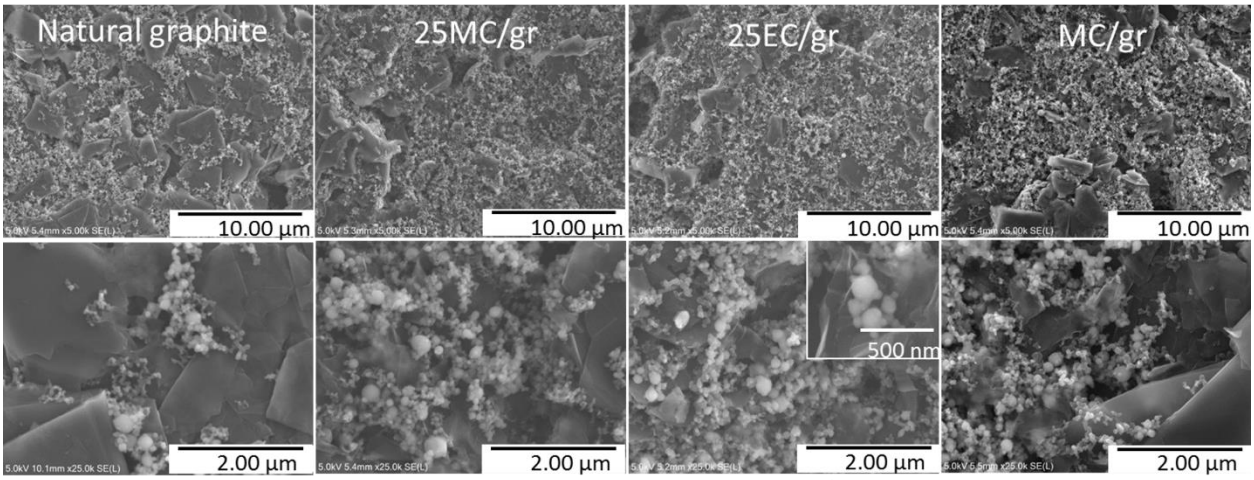

Fig. 9 SEM images of Si/graphite composites.

Composite anodes containing Si with active loading of 6.5-6.7 mg/cm^2 demonstrate improved capacity compared with that of graphite (Fig. 10, Table 2). Composite of unmodified natural graphite with Si showed the lowest capacity among all composites reaching only 400 mAh/g after 40 cycles while the first cycle capacity was only 54 mAh/g and coulombic efficiency was 49.6%. The capacity after 100 cycles was only 328mAh/g (82% capacity retention) which is even lower

than the capacity of natural graphite without any Si. The behavior of Si/natural graphite composite supports our assumption on the lack of compatibility between highly hydrophobic graphite, hydrophilic binder and Si. Composites of Si with modified graphite show much more improved cycling behavior – all of them have higher coulombic efficiency of the first cycle (82.9% – 25MC/gr, 82.3% – 25EC/gr, and 83.3 – MC/gr;) and more stable cycling. 25MC/gr shows the highest maximal capacity of 480 mAh/g (after 30 cycles) however capacity retention is only 77% after 100 cycles (370 mAh/g). 25EC/gr shows the most stable cycling and excellent capacity retention: it reaches 471 mAh/g after 45 cycles and has 99% capacity retention after 100 cycles (466 mAh/g).

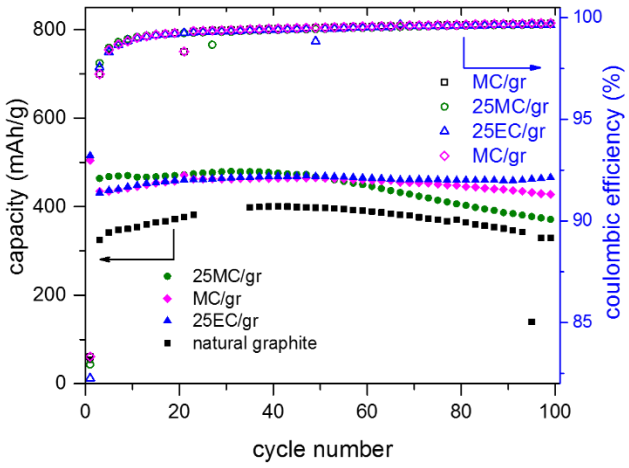

Fig. 10 Cycling performance of Si/graphite composites in Li-ion half cells. Active material loading 6.5-6.7 mg/cm^2 at C/12 rate

Improvement of the composite capacity with modified graphite is seen even more pronounced if one takes into consideration the capacity of individual graphite – modified graphite samples showed lower capacity than natural graphite but together with Si they provided capacity of up to 480 mAh/g which means increased contribution of Si into the total capacity of the composite.

Nominal capacity of silicon might be roughly estimated by subtracting capacity of corresponding graphite from the capacity of the composite (Table 2). Even though this method does not give the precise value of Si capacity it can however be used for estimation of overall trend. Si in composite with natural graphite showed the lowest capacity – 703 mAh/g, while it showed two times higher capacity using modified graphite; Si reached the highest capacity with 25MC/gr (1664 mAh/g).

We have also prepared composite electrodes with lower loading (2.8-3.2 mg/cm^2) of active material to study their rate capability. As it was expected the cycling behavior of all materials was improved substantially compared to electrodes with higher active material's loading (Fig. 11, Table 2) which is a result of better accessibility of active material by electrolyte and therefore faster and more efficient lithiation-de-lithiation reactions. The highest capacity was demonstrated by composite of Si with 25MC/gr – the maximal capacity reached was 565 mAh/g and after 100 cycles capacity was still as high as 534 mAh/g which is 95% of maximal capacity. Nominal capacity of Si in this composite was calculated to be 2326 mAh/g which is the highest among all composites. Taking into account substantial content of electrochemically-inactive silicon dioxide in the Si nanopowder the achieved capacity is close to "practical" capacity of silicon which is 3579 mAh/g [44]. When used with other modified graphite, Si also showed higher capacity compared to composite with unmodified natural graphite (25EC/gr – 2102 mAh/g, MC/gr – 2271 mAh/g, graphite – 1991 mAh/g) thus demonstrating positive effect of surface modification with cellulose-derived carbon coating.

Composite of Si with 25MC/gr shows excellent rate capability as well – it shows twice higher capacity at rate 1C (0.8A/g) than Si/natural graphite composite (171.3 mAh/g for 25MC/gr against 85.7mAh/g for natural graphite).The first cycle coulombic efficiency was also improved in all composites containing modified graphite (Table 2). We believe that the electrochemical

performance of composites can be further improved if the process of grinding of synthesized 25MC/gr would be optimized to yield more uniform particle distribution leading to better mechanical and structural properties of electrodes.

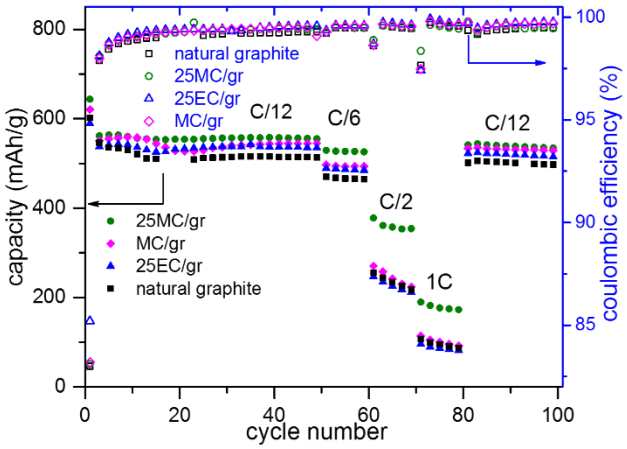

Fig. 11 Cycling performance of Si/graphite composites in Li-ion cells. Active material loading 2.8-3.2 mg/cm^2 at C/12 rate

Differential capacity (dQ/dV) curves and charge/discharge curves of composite electrodes show peaks characteristic of lithiation/delithiation of both graphite and Si (Fig. 12) [33, 45]. Sharp and well-defined peaks in the dQ/dV curves and plateaus in corresponding voltage curves during lithiation in the regions around 0.2, 0.1 and 0.07 V (for the 1st cycle - at 0.17, 0.09, 0.05 V) are typical for Li intercalation into graphite while its deintercalation occurs at 0.11, 016, 0.23 V [33]. Initial Si lithiation is supposed to start at 0.1V which overlaps with graphite lithiation, while the first delithiation of Si was observed at 0.44 V. Upon further cycling Si lithiation peaks were observed at 0.25V while delithiation peaks were observed around 0.45V and 0.27V. Also worth mentioning that the expected Si delithiation peak at 0.1 was obscured by graphite delithiation peak

[45]. Except in the first cycle there was no change in the shape of peaks assigned to Si lithiation/delithiation with cycling which points to reversibility of electrochemical reactions.

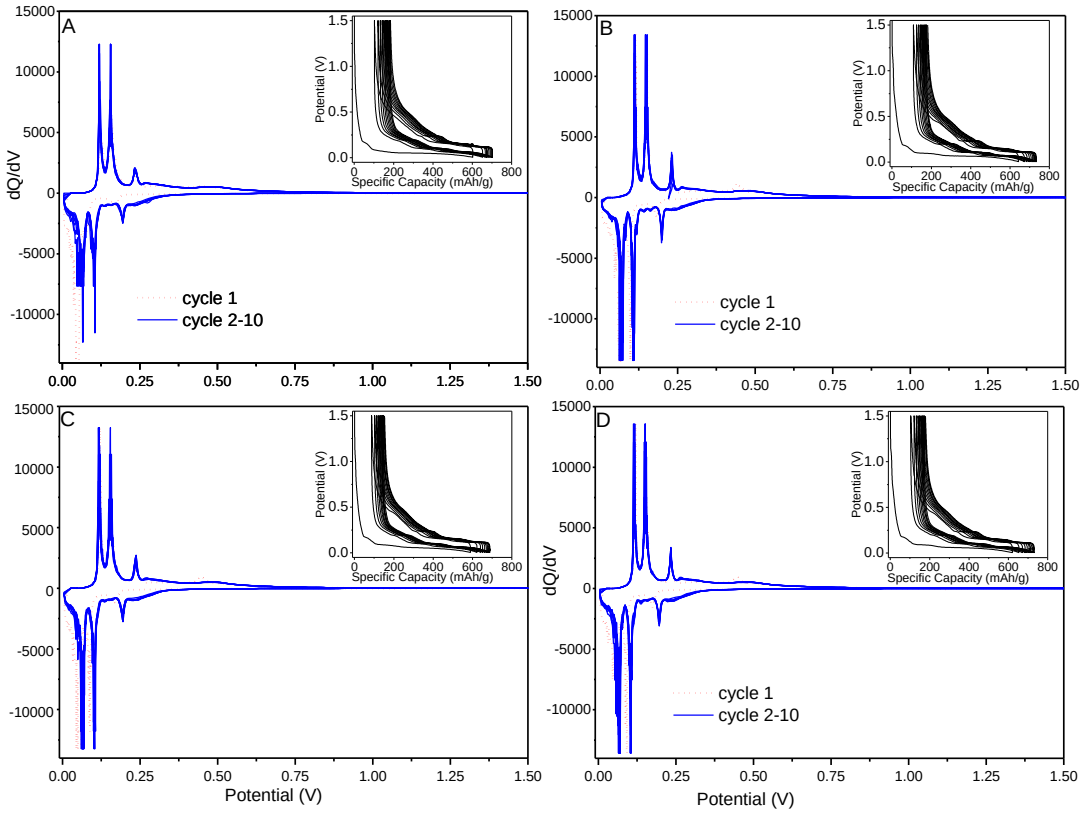

Fig. 12 Differential capacity plots for Si containing composites. Inset: voltage curves of corresponding electrodes. a – natural graphite, b – 25MC/gr, c – 25EC/gr, d – MC/gr.

The obtained results clearly show positive effect of both graphite exfoliation and modification with amorphous carbon on enhancing compatibility with silicon. Despite high surface area of 25MC/gr, its composite electrode does not show decrease in reversible capacity which might be compensated

for by decreasing the irreversible capacity of Si caused by better accommodation of Si particles by modified graphite and porous amorphous carbon.

3. Conclusions

In the present work, we modified the surface of graphite in order to make it compatible with Si nanoparticles to prepare high capacity composite anodes for Li-ion batteries. Modification of graphite was carried out in two steps: first, graphite was partially exfoliated in a solution of cellulose derivatives (methylcellulose or ethylcellulose), then it was heat treated in an inert atmosphere in order to carbonize the polymers into a conductive carbon layer. It was found that the surface of graphite is formed from graphene conductive networks and thin, oxygen-rich, amorphous carbon layers that is believed to be the cause of the increase compatibly with Si nanoparticles. Li-ion battery testing showed that Si/graphite composite give superior capacity compared to anodes containing unmodified graphite: it developed a capacity of 565mAh/g with 95% capacity retention after 100 cycles. Composite anode also showed excellent rate capability – it had twice higher capacity at 1C rate than Si/natural graphite composite. We believe that the process is straightforward and flexible enough to allow the preparation of other anode materials for Li-ion and other batteries.

4. Experimental section

4.1 Materials

Graphite, natural (flakes, ~325 mesh, 99.98% carbon content) was purchased from Alfa Aesar. Silicon nanopowder (<100 nm particle size, ≥ 98% trace metals basis), sodium carboxymethyl cellulose (NaCMC, average Mw ~ 90000, 0.7 carboxymethyl groups per anhydroglucose unit),

methyl cellulose (MC, average Mn ~ 40000), ethyl cellulose (EC, extent of labelling 48% ethoxyl), ethylene carbonate (anhydrous, 99%), and diethyl carbonate (anhydrous, 99%+), $LiPF_6$ (battery grade, ≥ 99.99% trace metals basis) were purchased from Sigma-Aldrich and used as received. Monofluoroethylene carbonate was purchased from Solvay and used as received. Double deionized water (MiliQ) was used for preparation of water solutions and dispersions. Carbon Super P was purchased from Timcal and stored at 90˚C prior to use.

4.2 Modification of natural graphite samples

3wt/vol% aqueous solution of MC and acetone solution of EC were first prepared at room temperature and left overnight. Then graphite was added to solutions and the weight ratio of graphite to polymer was 10:3. Graphite dispersions were put into an ice-cooled sonicator (VWR, B2500A-MT) and kept sonicating at 42(±2.5) kHz and 85W for 25 hours. Prepared graphene/graphite dispersions were further dried: the dispersion in EC was air dried and the dispersion in MC was freeze-dried. To study the influence of liquid exfoliation on graphite electrochemical performance, a control non-sonicated MC/graphite composite was prepared (10:3 graphite: polymer weight ratio).

Dried polymer/graphene/graphite composites were carbonized in a tube furnace at 800˚C for 1 hour (in nitrogen flow). Heating rate was 5˚C/min. After carbonization, the samples were left to cool down to room temperature before they were taken out in order to avoid excessive oxidation. Obtained samples were manually ground in agate mortars before further use. The final carbonized composites were named as 25MC/gr, 25EC/gr (graphite exfoliated for 25 hours in MC or EC solution correspondingly), MC/gr (graphite was mixed with MC solutions without exfoliation).

4.3 Determination of Graphene Concentration in Dispersion by Spectrophotometry

To measure the graphene concentration, aliquots of graphene/graphite dispersions were drawn at room temperature (22 (±1) ˚C) and were centrifuged using the Eppendorf Centrifuge 5702 at 3000 rpm (relative centrifugal force 1400 G) during 2 hours. Centrifuged dispersions were left overnight prior to further measurements, then they were diluted 100 times with corresponding solvent.

Measurement of optical absorbance was performed in Cole Parmer 1200 spectrophotometer at 660 nm in polystyrene (for water dispersions) or quartz (for acetone dispersions) cuvettes (1 cm optical pathlength).

Concentration (C) was measured as:

$C=dA/l\ \alpha$, [37]

where: ***d*** is dilution, ***A*** is optical absorbance, ***l*** is optical pathlength (m), and ***α*** is optical absorption coefficient ($Lg^{-1}m^{-1}$).

α for graphene dispersions in MC and EC was taken to be the same as the one for graphene dispersions in NaCMC solution ($Lg^{-1}m^{-1}$) which was measured by us previously to be 3155 $Lg^{-1}m^{-1}$ [34].

4.4 Characterization of samples

Transmission electron microscopy (TEM) of acetone dispersions casted on copper grids covered with holey carbon film was performed with FEI Titan 3 80-300 at 300 kV acceleration voltage.

The X-ray diffraction (XRD) patterns were recorded by Bruker D8 Advance diffractometer equipped with Våntec-1 detector. Radiation was generated with an X-ray tube with a Cu anode (Kα radiation, λ=1.54184 Å) at 40 kV and 40 mA. The 2θ range was 10-60˚, and the resolution

was 0.05˚ with 3s averaging time per step. Phase analysis was performed using ICDD PDF-2 databases (release 2008).

The morphology of the as-prepared composites was investigated with Scanning Electron Microscopy (SEM) using a Hitachi SU5000 in the secondary electron mode and acceleration voltage 5-10kV. Samples were mounted onto sample holders with double-sided conductive tape, no conductive coating was applied.

Thermal gravimetric analysis (TGA) of samples was performed by Hi-Res TGA 2950 Thermogravimetric Analyzer (TA instruments). Samples were first kept at 100˚C for 1 hour in order to remove adsorbed water, then they were heated to 800 ˚C at 5˚C/min heating rate, then samples were kept for 1 hour at this temperature. Nitrogen was used as a carrying gas.

Specific surface area was measured from low temperature nitrogen sorption/desorption at 77K performed with ASAP 2020 Accelerated Surface Area and Porosity System (Micromeritics) using Brunauer-Emmett-Teller method. Outgassing of samples prior to measurements was performed in vacuum at 150 ˚C during 4 hours.

XPS spectra were recorded with Kratos Axis Ultra spectrometer using a monochromated Al X-ray source. Beam aperture size was 300×700 μm. Pass energy for survey spectra was 160eV, for high resolution spectra C1s spectra - 20 eV. Resolution for survey spectra was 1 eV, and 0.1 eV for C1s spectra. Data processing was carried out with CasaXPS software, charge correction was performed by assigning the position of C1s peak to 284.8 eV.

4.5 Electrochemical testing

Electrochemical performance was studied in half cells versus metallic Li. The electrode was prepared by mixing modified graphite, Si, Carbon Super P with NaCMC solution in water (5.0 wt%). The final electrode composition was 10% Si, 78% graphite, 2% CSP and 10% NaCMC or 88% graphite, 2% CSP and 10% NaCMC. Homogeneous slurry was prepared in planetary centrifugal mixer THINKY ARE-310 operating at 2000 rpm. The slurry was casted onto a copper foil current collector (cleaned with 2.5% HCl solution) using an automated doctor-blade spreader (thickness 250 or 150 μm). The cast was dried in air overnight, then it was roller pressed at 700 kPa and then discs (d=12.5 mm) were punched out and kept at least 24 hours in the vacuum oven at 80˚C prior to cell assembly and stored there in order to minimize the oxidation of Si.

Specific weight of active material was 6.5-6.7 mg/cm^2 when slurries were spread with 250 μm doctor blade and 2.8-3.2 mg/ cm^2 when slurries were spread with 150 μm doctor blade.

2325-type coin cells, purchased from the National Research Council of Canada, were assembled under argon in the glove box. A lithium disc (d=16.5 mm) was used as a negative electrode (counter electrode and reference electrode); 80 μl of 1 M $LiPF_6$ solution in ethylene carbonate: diethyl carbonate (3:7 volume ratio) containing 10 vol% of monofluoroethylene carbonate was used as an electrolyte. A double layer of the microporous polypropylene film (30 μm thick, Celgard 2500) was used as a separator. Capacity measurements were performed by galvanostatic experiments at multichannel Arbin battery cycler (BT2000). The working electrode was first discharged (lithiated) down to 0.005 V and then charged (delithiated) to 1.500 V galvanostatically at currents corresponding to charge or discharge in 12, 6, 2 or 1 h (C/12, C/6, C/2 or 1C).

Acknowledgments

The authors thank Natural Resources Canada for financial support through the Program of Energy Research and Development (Electric Mobility program). The authors wish to thank David Kingston for valuable advice on SEM operation, Oltion Kodra for recording of XPS spectra and Dr. Martin Couillard for TEM micrographs.

References

[1] A.M. Wilson and J.R. Dahn, Lithium insertion in carbons containing nanodispersed silicon, *J. Electrochem. Soc.*, 1995, **142**, 326–332.

[2] C.C. Nguyen, T. Yoon, D.M. Seo, P. Guduru and B.L. Lucht, Systematic investigation of binders for silicon anodes: interactions of binder with silicon particles and electrolytes and effects of binders on solid electrolyte interphase formation, *ACS Appl. Mater. Interfaces*, 2016, **8**, 12211–12220.

[3] M. Ge, J. Rong, X. Fang and C. Zhou, Porous doped silicon nanowires for lithium ion battery anode with long cycle life, *Nano Lett.*, 2012, **12**, 2318–2323.

[4] C. Erk, T. Brezesinski, H. Sommer, R. Schneider and J. Janek, Toward silicon anodes for next-generation lithium ion batteries: a comparative performance study of various polymer binders and silicon nanopowders, *ACS Appl. Mater. Interfaces*, 2013, **5**, 7299–7307.

[5] A. Casimir, H. Zhang, O. Ogoke, J.C. Amine, J. Lu and G.Wu, Silicon-based anodes for lithium-ion batteries: effectiveness of materials synthesis and electrode preparation *Nano Energy*, 2016, **27**, 359–376.

[6] M.R. Zamfir, H.T. Nguyen, E. Moyen, Y.H. Lee and D. Pribat, Silicon nanowires for Li-based battery anodes: a review, *J. Mater. Chem. A*, 2013, **1**, 9566–9586.

[7] Y. Ru, D.G. Evans, H. Zhu and W. Yang, Facile fabrication of yolk-shell structured porous Si-C microspheres as effective anode materials for Li-ion batteries, *RSC Adv.*, **2014**, 4, 71–75.

[8] J. Liu, P. Kopold, P.A. van Aken, J. Maier and Y. Yu, Energy storage materials from nature through nanotechnology: a sustainable route from reed plants to a silicon anode for lithium-ion batteries ,*Angew. Chem. Int. Ed*, 2015, **54**, 9632–9636.

[9] H. Wu, N. Du, X. Shi and D. Yang, Rational design of three dimensional macroporous silicon as high performance Li-ion battery anodes with long cycle life, *J. Power Sources*, 2016, **331**, 76–81.

[10] K. Xu, L. Ben, H. Li and X. Huang, Unique silicon-based nanosheets synthesized by the topochemical reaction as anodes for lithium ion batteries, *Nano Res.*, 2015, **8**, 2654–2662.

[11] J. Chen, L. Bie, J. Sun and F. Xu, Enhanced electrochemical performances of silicon nanotube bundles anode coated with graphene layers, *Mater. Res. Bull.*, 2016, **73**, 394–400.

[12] R. Krishnan, R. Mukherjee, T.M. Lu, and N. Koratkar, Nano-engineered silicon anodes for lithium-ion rechargeable batteries in Y. Abu-Lebdeh and I. Davidson (eds), *Nanotechnology for Lithium-Ion Batteries,* Springer, New York, 2013, 43–66.

[13] T. Yoon, C.C. Nguyen, D.M. Seo and B.L. Lucht, Capacity Fading Mechanisms of Silicon Nanoparticle Negative Electrodes for Lithium Ion Batteries, J. *Electrochem. Soc.*, 2015, **162**, A2325–A2330.

[14] J.K. Lee, C. Oh, N. Kim, J.Y. Hwang and Y.K. Sun, Rational design of silicon-based composites for high-energy storage devices, *J. Mater. Chem. A*, 2016, **4**, 5366–5384.

[15] Y. Ma, R. Younesi, R. Pan, C. Liu, J. Zhu, B. Wei and K. Edström, Constraining Si particles within graphene foam monolith: interfacial modification for high-performance Li^+ storage and flexible integrated configuration, *Adv. Funct. Mater*., 2016, **26**, 6797–6806.

[16] M. Tokur, H. Algul, S. Ozcan, T. Cetinkaya, M. Uysal and H. Akbulut, Closing to scaling-up high reversible Si/rGO nanocomposite anodes for lithium ion batteries, *Electrochim. Acta.*, 2016, **216**, 312–319.

[17] L.Y. Yang, H.Z. Li, J. Liu, Z.Q. Sun, S.S. Tang and M. Lei, Dual yolk-shell structure of carbon and silica-coated silicon for high performance lithium-ion batteries, *Sci. Rep.*, 2015, **5**, DOI: 10.1038/srep10908.

[18] S. Sim, P. Oh, S. Park and J. Cho, Critical thickness of SiO_2 coating layer on core@shell bulk@nanowire Si anode materials for Li-ion batteries, *Adv. Mater*., 2013, **25**, 4498–4503.

[19] Y.S. Hu, R. Demir-Cakan, M.M. Titirici, J.O. Müller, R. Schlögl, M. Antonietti and J. Maier, Superior Storage Performance of a Si@SiO_x/C Nanocomposite as Anode Material for Lithium-Ion Batteries, *Angew. Chem. Int. Ed.*, 2008, **47**, 1645–1649.

[20] S.J. Kim, M.C. Kim, S.B. Han, G.H. Lee, H.S. Choe, D.H. Kwak, S.Y. Choi, B.G. Son, M.S. Shin and K.W. Park., 3D flexible Si based-composite (Si@Si_3N_4)/CNF electrode with enhanced cyclability and high rate capability for lithium-ion batteries, *Nano Energy*, 2016, **27**, 545–553.

[21] Y.Bai, D. Yan, C. Yu, L. Cao, C. Wang, J. Zhang, H. Zhu, Y.S. Hu, S. Dai, J. Lu and W. Zhang, Core-shell Si@TiO_2 nanosphere anode by atomic layer deposition for Li-ion batteries, *J. Power Sources*, 2016, **308**, 75-82.

[22] N. Liu, H. Wu, M.T. McDowell, Y. Yao, C. Wang and Y. Cui, A Yolk-Shell design for stabilized and scalable Li-ion battery alloy anodes, *Nano Lett.*, 2012, **12**, 3315–3321.

[23] S.H. Choi, D.S. Jung, J.W. Choi and Y.C. Kang, Superior lithium-ion storage properties of Si-based composite powders with unique Si@Carbon@Void@Graphene configuration, *Chem. Eur. J.*, 2015, **21**, 2076–2082.

[24] J. Yang, Y.X. Wang, S.L. Chou, R. Zhang, Y. Xu, J. Fan, W.X. Zhang, H.K. Liu, D. Zhao and S.X. Dou, Yolk-shell silicon-mesoporous carbon anode with compact solid electrolyte interphase film for superior lithium-ion batteries, *Nano Energy*, 2015, **18**, 133–142.

[25] Z.P. Guo, E. Milin, J.Z. Wang, J. Chen and H.K. Liu, Silicon/disordered carbon nanocomposites for lithium-ion battery anodes, J. Electrochem. Soc., 2005, **152**, A2211–A2216.

[26] Y. Liu, Z.Y. Wen, X.Y. Wang, A. Hirano, N. Imanishi and Y. Takeda, Electrochemical behaviors of Si/C composite synthesized from F-containing precursors, *J. Power Sources*, 2009, **189**, 733–737.

[27] C.H. Yim, F. Courtel and Y. Abu-Lebdeh, A high capacity silicon-graphite composite as anode for lithium-ion batteries using low content amorphous silicon and compatible binders, *J. Mater. Chem. A.*, 2013, **1**, 8234–8243.

[28] J.L. Gómez-Cámer, C. Bünzli, M.M. Hantel, T. Poux and P. Novak, On the correlation between electrode expansion and cycling stability of graphite/Si electrodes for Li-ion batteries. *Carbon*, 2016, **105,** 42–51.

[29] Z.J. Han, K. Yamagiwa, N. Yabuuchi, J.Y. Son, Y.T. Cui, H. Oji, A. Kogure, T. Harada, S. Ishikawa, Y. Aoki and S. Komaba, Electrochemical lithiation performance and

characterization of silicon-graphite composites with lithium, sodium, potassium, and ammonium polyacrylate binders, *Phys. Chem Chem. Phys.*, 2015, **17**, 3783.

[30] C.H. Yim, S. Niketic, N. Salem, O. Naboka and Y. Abu-Lebdeh, Towards improving the practical energy density of Li-ion batteries: optimization and evaluation of silicon:graphite composites in full cells, *J. Electrochem. Soc.*, 2017, **164**, A6294–A6302.

[31] N. Nitta and G. Yushin, High-capacity anode materials for lithium-ion batteries: choice of elements and structures for active particles, *Part. Part. Syst. Charact.*, 2014, **31**, 317–336.

[32] K. G. Gallagher, S. E. Trask, C. Bauer, T. Woehrle, S. F. Lux, M. Tschech, P. Lamp, B.J. Polzin, S. Ha, B. Long, Q. Wu, W. Lu, D.W. Dees and A. N. Jansen, Optimizing areal capacities through understanding the limitations of lithium-ion electrodes, *J. Electrochem. Soc.*, 2016, **163** A138–A149.

[33] P. Novák, D. Goers and M.E. Spahr, Carbon materials in lithium-ion batteries, in *Carbons for Electrochemical Energy Storage and Conversion Systems,* E. Frackowiak and F. Béguin (eds), Taylor and Francis Group, Boca Raton, FL, 2010, chapter 7, 263–328.

[34] O. Naboka, C.H. Yim and Y. Abu-Lebdeh, Graphene/Na carboxymethyl cellulose composite for Li-ion batteries prepared by enhanced liquid exfoliation, *Mater. Sci. Eng. B*, 2016, **213**, 41–50.

[35] O. Naboka, K. Rodriguez, A.F. Toomadj, A. Sanz-Velasco, G. Toriz, P. Lundgren, P. Enoksson and P. Gatenholm. Carbon nanofibers synthesized from electrospun cellulose for advanced material applications, *Materials Science Forum*, 2013, **730-732**, 903–908.

[36] V. Kuzmenko, O. Naboka, P. Gatenholm and P. Enoksson, Ammonium chloride promoted synthesis of carbon nanofibers from electrospun cellulose acetate, *Carbon*, 2014, **67**, 694–703.

[37] Y. Hernandez, V. Nicolosi, M. Lotya, F. M. Blighe, Z. Sun, S. De, I.T. McGovern, B. Holland, M. Byrne, Y.K. Gun'ko, J.J. Boland, P. Niraj, G. Duesberg, S. Krishnamurthy, R. Goodhue, J. Hutchison, V. Scardaci, A.C. Ferrari and J. Coleman, High-yield production of graphene by liquid-phase exfoliation of graphite, *Nat. Nanotechnol.*, 2008, **3**, 563–568.

[38] L. Pan, J. Chen, C. Wan, H. Ren, H. Zhai, and J. Zheng, Investigating the environmental impact of pyrolysis volatiles of printing paper under a nitrogen atmosphere, *Cellulose Chem. Technol.*, 2015, **49**, 863-871.

[39] A.Ciesielski and P. Samori, Graphene via sonication assisted liquid-phase exfoliation, *Chem. Soc. Rev.*, 2014, **43**, 381–398.

[40] R.I.R. Blyth, H. Buqa, F.P. Netzer, M.G. Ramsey, J.O. Besenhard, P. Golob and M. Winter, XPS studies of graphite electrode materials for lithium ion batteries, *Appl. Surf. Sci.*, 2000, **167**, 99–106.

[41] K. Zaghib, X. Song, A. Guerfi, R. Rioux and K. Kinoshita, Purification process of natural graphite as anode for Li-ion batteries: chemical versus thermal, *J. Power Sources*, 2003, **119-121**, 8–15.

[42] T. Susi, T. Pichler and P. Ayala, X-ray photoelectron spectroscopy of graphitic carbon nanomaterials doped with heteroatoms, *Beilstein J. Nanotechnol,* 2015, **6**, 177–192.

[43] R. Schlögl and H.P. Boehm, Influence of crystalline perfection and surface species on the X-ray photoelectron spectra of natural and synthetic graphites, *Carbon*, 1983, **21**, 345–358.

[44] M.N. Obrovac and L.Christensen, Structural changes in silicon anodes during lithium insertion/extraction, *Electrochem. Solid-State Lett.*, 2004, **7**, A93–A96.

[45] M.N Obrovac, L.J. Krause, Reversible cycling of crystalline silicon powder, *J. Electrochem. Soc.*, 2007, **154**, A103–A108.